Model of the Human Cardiovascular System

Tomer Berlinski, Beatrice Costa, Manuel Ehrlich, Elena Moral Sánchez

June 1, 2022

Abstract

The aim of this study is to find a suitable mathematical model to describe the cardiovascular system as a compartmental model with 14 interconnected compartments, and to numerically integrate said equations in order to obtain a meaningful and reasonably accurate solution.
This system is examined through a combination of lumped 0D models to represent heart chambers, valves, blood vessels and the relation between them. Described with a system of ordinary differential and algebraic equations for pressure, flow rate and volume, the model aims to simulate the blood flow through pulmonary and systemic circulation, and the heart.
The system is then solved numerically using different methods and adapting them to the issues that the model presents. At the end some factors to measure the performance are introduced to compare the numerical implementations.
The ultimate goal of this study is to observe how parameters such as elasticity and heart rate, which vary due to aging or pathological conditions, influence the functionality of the heart.

1 Introduction

The importance, as well as the complexity, of modeling the cardiovascular system lies in its essential function for human life and its structure. Designed to supply every part of the body with blood, it relies on a gradient of pressure applied by the rhythmic contraction and relaxation of heart chambers, controlled by valves [8]. Besides, a satisfactory model would require a great number of variables to model the whole vascular network and its complex topology, leading to a very complex 3D system involving fluid dynamics. However, as shown by Fuyou Liang, Shu Takagi, Ryutaro Himeno and Hao Liu in their research, a satisfactory simplification can be achieved by the use of a less complex lumped model to describe the compartments [9]. This allows a simpler mathematical formulation and a faster numerical implementation. It is then only necessary to solve ordinary differential and algebraic equations for the 14 compartments taken into account, in order to model the behavior of blood pressure, volume and flow rate. Lastly, the resulting system will be solved numerically.

2 Cardiovascular Physiology: a brief overview

The cardiovascular system plays a vital role in the human body: it supplies the tissues with oxygen-rich blood, while carrying away waste. Its complex yet functional structure, which will be modeled in this study, consists of a closed loop of vessels which carry blood to and from the heart which, through rhythmic contractions and relaxations of its chambers, generates a pressure gradient, allowing therefore the circulation of blood.

The heart is divided in four chambers: two atria, which receive the blood from the veins, and two ventricles, which pump it into the arteries. In the *diastolic* phase, ventricles fill with blood due to atrial contraction; while the contraction of ventricles, which allows the blood to flow into the arteries through the pulmonary and aortic valves is denominated *systole*. This process generates the pressure gradient which accounts for the circulation of blood through the whole system.

However, the heart is not the only part of the system that is able to contract: for example, arteries coating is formed by three layers, the middle of which (*tunica intermedia*) is composed by muscle tissue. Therefore, the blood volume is not everywhere fixed and it varies in time. The multi-layer coating of blood vessels is differentiated based on their function: in the case of capillaries, which *close the loop* [9] by leading the blood from arteries to veins, the only present layer is composed of endothelial tissue, allowing thus the exchange by diffusion of waste products and oxygen with the surrounding tissues.
In case of increased cardiac activity, e.g. due to physical effort, the consumption of oxygen by tissues rises because of physiological mechanisms such as higher cardiac frequency and arterial dilation.
Due to the continuous expansion and contraction of the tissues involved, a parameter that plays an important role is the elasticity: it represents the ability of the compartments to return to their original volume after expanding[5]. An observed clinical effect of the decrease in elasticity is therefore the reduced pumping power of the heart, caused for instance by aging.

The aim of this study is thus to find a satisfactory mathematical description of the system, involving the following variables and parameters: pressure, volume, flow rate, inertia, viscosity and a simulation of the effect of the valves [8].

3 Mathematical Model

3.1 Model Idea

Despite the complexity of the heart and of the whole cardiovascular system, the following simplification can be made: in order to simulate basic phenomena, e.g. pulse wave or valve regulation, the system can be approximated to a network

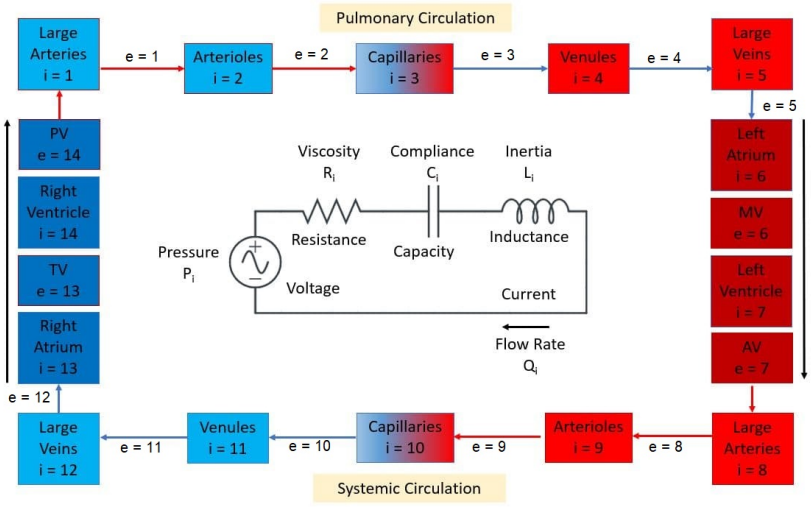

Figure 1: Illustration of the compartment model used for the Cardiovascular System and its equivalence as a RLC Circuit.

of compartments by using a 0D model [9].

In order to achieve this, the system is divided in compartments connected by edges using a lumped parameter model, which allows to find ordinary differentiable and algebraic equations for the blood volume, pressure, flow rate and the opening coefficients of the valves [9]. Such equations are then solved numerically.

3.2 Parallel with electronics

At first glance, the nature of the system would call for equations whose structure resembles those of fluid dynamics [10]. The blood would thus be described in most vessels as a viscous fluid which experiences laminar flow due to low Reynolds numbers; in proximity of valves and in the biggest arteries there would be turbulent effects due to high Reynolds numbers [10]. However, a more suitable mathematical description can be devised by drawing a parallel between the quantities that describe the compartments and edges of the model and an electric circuit. Analyzing such dynamics in a concentrated parameter study would efficiently describe the behavior of valves by modeling them in a simple way as diodes (due to their role in ensuring a one-way circulation). However, the turbulence effect near them is also considered in this model [8].

3.3 Qualitative justification

The comparison is especially sound because of the similarity between the physical meanings of the involved parameters and variables:

- Pressure and Voltage: Both have the function of driving the flow of, respectively, blood and charges through the circuit. Hence, the description of pressure is similar to Ohm's and Kirchhoff's laws.
- Viscosity and Resistance: Their role is to oppose the flow of blood and charges by internal friction of the fluid in the first case, and by physical collisions in the latter.
- Compliance and Capacity: In the first case, it describes the ability of heart chambers and vessels to expand under the pressure gradient, while in the latter it describes the ability of the capacitor to store excess charge, under the potential difference.
- Inertia and Inductance: Both of them act as a "tendency of the circuit to oppose changes in flux", as described in the electric circuit case by Lenz and Oersted's laws.
- Blood Flow and Current: Both of them represent the stream of particles that move through a closed loop

As introduced in the previous paragraphs, a valid model would be composed of equations that mimic the description of a RLC circuit. Since the cardiovascular system is a closed loop, mass and momentum conservation laws can be applied to flow rate and volume [9]. Similarly, the pressure gradient can be structured analogously to Kirchhoff's Voltage law, with terms that account for inertia, viscosity and turbulence effect.

3.4 Mathematical description of the system

The model can be therefore formulated using 46 equations. Note that for connections between heart compartments where there is a valve, it is necessary to take into account the turbulence created by the valve. This effect can be neglected in case of absence of a valve, as aforementioned in the discussion of Reynolds numbers [8], [10].

- 14 ordinary differential equations for the blood volume $V_i(t)$ in compartment i with inlet and outlet edges $e-1$ and e, respectively.

$$\dot{V}_i(t) = Q_{e-1}(t) - Q_e(t) \tag{1}$$

- 10 ordinary differential equations for the flow rate $Q_e(t)$ at edge e between compartments i and $i+1$, not connected by any valve:

$$L_e\dot{Q}_e(t) = P_i(t) - P_{i+1}(t) - R_eQ_e(t) \tag{2}$$

- 4 ordinary differential equations for the flow rate $Q_e(t)$ at edge e between heart compartments i and $i+1$, connected by a valve:

$$L_e\dot{Q}_e(t) = P_i(t) - P_{i+1}(t) - R_eQ_e(t) - B_eQ_e(t)\,|Q_e(t)| \tag{3}$$

Where L_e is the inertia, R_e the viscosity and B_e the turbulence. Note that the absolute value in the turbulence term introduces a point of non-differentiability in the model.

- 4 ordinary differential equations for the opening coefficient $O_e(t)$ at edge e containing a valve.

$$C_{d,e}\dot{O}_e(t) = 0.5\left[1 + \tanh\left(C_{v,e}(P_i(t) - P_{i+1}(t))\right)\right] - O_e(t) \tag{4}$$

Where $C_{d,i}, C_{v,i}$ are the dynamic characteristics and ejection velocity for compartment i.

- 10 algebraic equations for the pressure inside a non-heart compartment i:

$$C_i P_i(t) = V_i(t) - V_{0,i} \tag{5}$$

- 4 algebraic equations for the pressure inside a heart compartment i:

$$\left[1 - 0.0005(Q_{e-1}(t) - Q_e(t))\right] P_i(t) = E_i(t)(V_i(t) - V_{0,i}) \tag{6}$$

Where $V_{0,i}$ is the dead volume and $E_i(t)$ the elasticity function for heart chambers, defined as $E_i(t) = E_{A,i}e_i(t(\mod T)) + E_{B_i}$. Here T is the duration of a heartbeat, $E_{A,i}$ the amplitude and $E_{B,i}$ the basis [9]. The activation function $e_i(t)$ is defined differently in atria (7) or ventricles (8).

$$e_i(t) = \begin{cases} \frac{1}{2}\left[1 + \cos(\frac{\pi(t+T-t_{r,i})}{T_{rp,i}})\right], & \text{if } 0 \le t \le t_{r,i} + T_{rp,i} - T \\ 0, & \text{if } t_{r,i} + T_{rp,i} - T < t \le t_{c,i} \\ \frac{1}{2}\left[1 - \cos(\frac{\pi(t-t_{c,i})}{T_{cp,i}})\right], & \text{if } t_{c,i} < t \le t_{c,i} + T_{cp,i} \\ \frac{1}{2}\left[1 + \cos(\frac{\pi(t-t_{r,i})}{T_{rp,i}})\right], & \text{if } t_{c,i} + T_{cp,i} < t \le T \end{cases} \tag{7}$$

$$e_i(t) = \begin{cases} \frac{1}{2}\left[1 - \cos(\frac{\pi t}{T_{cp,i}})\right], & \text{if } 0 \le t \le T_{cp,i} \\ \frac{1}{2}\left[1 + \cos(\frac{\pi(t-T_{cp,i})}{T_{rp,i}})\right], & \text{if } T_{cp,i} < t \le T_{cp,i} + T_{rp,i} \\ 0, & \text{if } T_{cp,i} + T_{rp,i} < t \le T \end{cases} \tag{8}$$

Where $T_{cp,i}$ and $T_{rp,i}$ represent the duration of contraction and relaxation for the respective heart chamber and $t_{c,i}$, $t_{r,i}$ denote the start of contraction and relaxation.

Lastly, it is necessary to add a post-processing, which accounts for the valves effect on the flow rates. This is done by multiplying the new flow rate by the new opening coefficient at each respective valve, i.e. $Q_e(t) := O_e(t)Q_e(t)$. Note that by definition, $O_e(t) \in [0, 1]$, where value 1 corresponds to a completely open valve and 0, to a closed valve. Thus, a completely open valve does not alter the flow rate, while a completely closed valve absolutely blocks the flux.

4 Numerical Solution

To solve the system of ordinary differential equations, different explicit Runge-Kutta methods of order 3(2), 4(5) and 5(4) are implemented. An alternative would be to use implicit Runge-Kutta methods. However, they are computationally costly and it is possible to achieve the desired accuracy in the model with the explicit methods. After solving the ordinary differential equations system for each time point, the pressure is updated using the algebraic equations.

4.1 Runge-Kutta Method

A Runge-Kutta method requires knowing the solution at a time point and setting a step-size, denoted by t_{old} and dt respectively. Then the solution $\eta(t_{old}+dt)$ is computed at time point $t_{new} = t_{old} + dt$ via intermediate stages:

$$\eta(t_{old} + dt) = \eta(t_{old}) + \sum_{i=1}^{s} b_i K_i \tag{9}$$

where the intermediate stages are defined as [7]:

$$K_i = dt \cdot f\left(\eta(t_{old}) + \sum_{j=1}^{i-1} a_{i,j} K_j\right) \tag{10}$$

Where $\eta(t_{old})$ is the numerical solution at time t_{old}, f is the right hand side of the ordinary differential equations system, dt is the step size and $b_i, a_{i,j}$ are the coefficients of the so-called Butcher Tableau. A standard explicit Runge-Kutta method of order four has four intermediate steps, called stages. However, there are two issues to be solved in order to apply the Runge-Kutta method:

- It requires smoothness of the right-hand side of the ordinary differential equations system. Two strategies to deal with this issue have been developed in this study. Either by directly finding the points of non-differentiability using the method of Andersson-Björck or by *smoothing out* the right-hand side.

- A way to control the discretization error, which requires the knowledge of the true solution, which is unknown. With this aim, Fehlberg method is implemented and the higher order method solution is used as the *true* solution. Besides, an adaptive stepsize allows for an efficient local discretization error control.

4.2 Automatic step size control

Imposing a uniform mesh where the function is differentiable would not allow to control the discretization error. By implementing adaptivity, it is possible to set a certain error tolerance and compute for each step the maximum time step size such that the local discretization error is lower than the set tolerance.

The Fehlberg method is initially implemented, which combines two one-step methods of different orders of convergence 4 and 5 with a common step size. Just taking two additional stages and an appropriate Butcher Tableau yields the fourth order approximation of the solution $\eta(t)$ and in addition it is possible to extrapolate a numerical solution $\tilde{\eta}(t)$ of order five [4].

The higher order solution $\tilde{\eta}(t)$ can be used as an estimate of the exact solution. Given that the right-hand side of the ordinary differential equations system is piece-wise C^∞, Gragg's theorem combined with Taylor expansions can be applied to get an estimate of the local discretization error:

$$\text{err} = \|\eta(t_{old} + dt) - \tilde{\eta}(t_{old} + dt)\| \tag{11}$$

Note that if the time interval includes points of non differentiability, the method is not valid anymore and the adaptive step size strategy cannot be used. Instead, a root-finding method has to be applied.

For adaptive step size control, two control parameters are introduced: $f_{\max}$ and $f_{\min}$, the maximum and minimum increase factor, respectively. Besides, tol is the chosen error tolerance, and p is the order of convergence of the lower order method. It is then set $f_{\max} = 1.5, f_{\min} = 0.3$ [7]. Adaptive time-step control is then implemented in the following way:

1. Compute

   $\eta(t_{old} + dt)$ and $\tilde{\eta}(t_{old} + dt)$ with step size dt.

2. The estimated error is given by $\text{err} = \|\eta(t_{old} + dt) - \tilde{\eta}(t_{old} + dt)\|$

3. Compute the new step size:

$$dt_{new} = dt \cdot \min\left(f_{\max}, \max\left(f_{\min}, 0.9\left(\frac{\text{tol}}{\text{err}}\right)^{\frac{1}{p+1}}\right)\right) \tag{12}$$

4.a. If err $>$ tol, repeat steps 1.- 4. with the new step size instead, i.e. by assigning $dt = dt_{new}$.

4.b. If err $\leq$ tol, save dt_{new} and end the loop.

Note that the loop will only end when it is satisfied that the local discretization error is smaller than the tolerance. For an alternative version, see Appendix A.

4.3 Anderson-Björck Method

It is necessary to find the zeros of the heart flow rates, which correspond to the points of non-differentiability of the right-hand side function. To do so, the Anderson-Björck algorithm, which is a modified version of the *regula falsi* method with improved performance, is implemented [6].

Firstly, it is required to set a tolerance for the root detection, which here is set to be the same as for the local discretization error. Secondly, it is necessary

to implement a system that detects when the Runge-Kutta step included points of non-differentiablity and is therefore not valid. This is achieved by checking changes of sign between the old and new heart flow rates. Besides, it is necessary to set aside the cases where one of the extremes is already a root (according to the set tolerance). After this filter is carried out, the cases where the algorithm should be applied have been selected.

The algorithm estimates the root of a function within a bracketing interval. After each iteration, the bracketing interval is shrunk so that the real root is still within. The method stops when the estimated root is smaller than the set tolerance. Observe that in this case, this method is generalized to more than one function, since it is possible that more than one aforementioned case is selected. Thus, the a priori estimate becomes a vector of estimates, from which the minimum is selected and used for computing the new solution.

In this section $\eta_h(t)$ will denote the numerical solution of the heart flow rates which require root-finding. At the k^{th} iteration, the root is between two time points t_a and t_b and the algorithm gives an estimate of the root $\vec{t_c}$. The selected flow rate will be denoted by $Q_a := \eta_h(t_a)$ and $Q_b := \eta_h(t_b)$ with $t_a < t_b$ and the zero $Q_c := \eta_h(t_c)$. Initially it holds $Q_a := \eta_h(t_{old})$ and $Q_b := \eta_h(t_{new}) = Q_c$. At each iteration, Anderson-Björck consists of the following steps [6]:

1. Define $\vec{m}_i = \begin{cases} 1 - \dfrac{\vec{Q}_{c,i}}{\vec{Q}_{b,i}} & \text{, if } \vec{Q}_{c,i} < \vec{Q}_{b,i} \\ 0.5 & \text{, otherwise} \end{cases}$

2. Compute (component-wise) $\vec{t_{c,i}} = \dfrac{\vec{Q}_{b,i} t_a - \vec{m}_i \vec{Q}_{a,i} t_b}{\vec{Q}_{b,i} - \vec{m}_i \vec{Q}_{a,i}}$

3. Find the closest root and its respective index I_c:

$$dt_c := \min_i(\vec{t_{c,i}} - t_{old}) \qquad I_c := arg\min_i(\vec{t_{c,i}} - t_{old})$$

4. Apply Runge-Kutta method from t_{old} and stepsize dt_c to find a new solution which contains the estimated zero $\vec{Q}_c$.

5.a If $|\vec{Q}_c(I_c)| < tol$, save solution and finish.

5.b Else if $\vec{Q}_c(I_c)$, $\vec{Q}_a(I_c)$ share sign, repeat loop with $(\vec{Q}_a, dt_a) = (\vec{Q}_c, dt_c)$.

5.c Otherwise, repeat loop with $(\vec{Q}_b, dt_b) = (\vec{Q}_c, dt_c)$.

Observe that this last step allows the shrinking of the interval so that the real root remains always within.

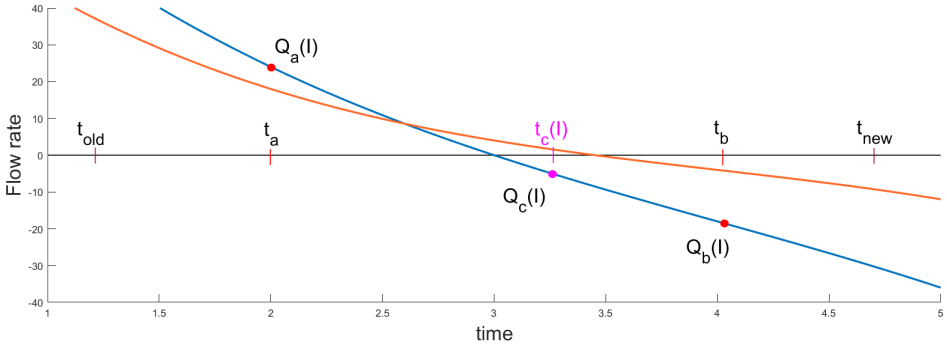

Figure 2: k^{th} iteration of Anderson-Björck in $[t_a, t_b]$ on two flow rates. Here the blue flow rate is selected for the root estimate $t_c(I)$, since it has the closest root to t_{old}.

4.4 *Smoothing* the right-hand side

An alternative to avoid the issue of non-smoothness in the right-hand side is to use a smooth substitute to the absolute value function. With that aim, the following family of functions $\{h_k\}_k$ is used:

$$h_k(x) = \sqrt{x^2 + 10^{-k}} \tag{13}$$

where $h_k \in C^\infty(R)$, for all k. The point-wise error is given by the Taylor series expansion at $x = 0$ of the smooth approximation:

$$e(x,k) = -|x| + 10^{-k/2} + \frac{10^{k/2}x^2}{2} - \frac{10^{3k/2}x^4}{8} + O(x^5) \quad \forall k \tag{14}$$

Clearly, the maximum error is $10^{-k/2}$ and it is reached at $x = 0$, thus in the points of non-differentiability. Besides, the log-log plot of the L^2-norm error for $x \in [-10^{-4}, 10^{-4}]$ shows that the L^2-norm error decreases exponentially.

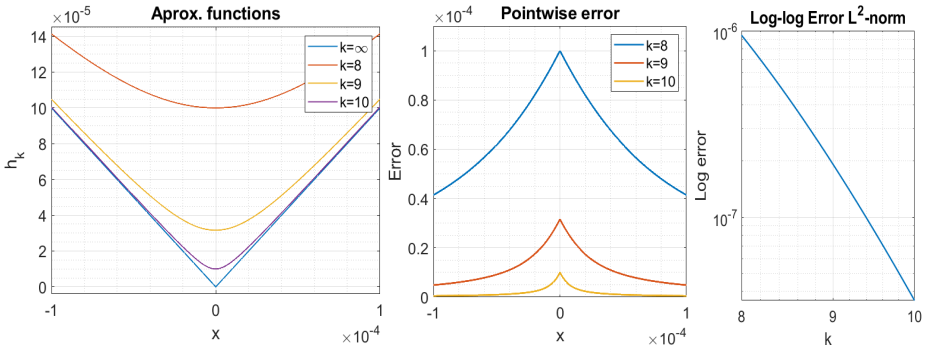

Figure 3: Left: $h_k(x)$. Center: Point-wise error. Right: Log-log plot of L^2-error.

4.5 Comparison between methods

In order to compare the performance of different methods, three diagnostic parameters have been introduced: dt_{mean}, $\text{bjoerck}_{\text{mean}}$ and $\text{adapt}_{\text{mean}}$. They correspond to the average step size, the average number of iterations of Anderson-Björck algorithm (when it is applied) and the average number of iterations of the adaptive time step loop, respectively. The average step size measures how efficient a method is and together with the step size evolution plot, it allows to do a performance comparison. The other two parameters can be used to set a tolerance such that there exists a balance between accuracy and speed. In the plots it has been set to 10^{-4}. Moreover, $\text{adapt}_{\text{mean}}$ is also a tool to adjust the fluctuation control parameters $f_{\max}$ and $f_{\min}$. The values of the diagnostic parameters can be found in Table 1.

With regard to the methods, the Cash-Karp method is firstly taken into account, which has a different Butcher Tableau than the Fehlberg method, but it similarly employs six stages to obtain a fourth order approximate solution and an extrapolated fifth order solution for error estimation [2]. The Dormand-Prince method, which employs an extra stage, was subsequently introduced. In the Fehlberg and Cash-Karp method, the Butcher Tableau coefficients are set to minimise the error for the fourth order approximate solution [2] [4]. On the contrary, the Dormand-Prince uses the extra evaluation to minimise the error for the fifth order approximate solution [3]. For this reason, the fifth order solution is used as the update in our MATLAB implementation. Finally, a simpler method has been checked: the Bogacki-Shampine method employs four stages to obtain a third order method with second order extrapolated solution [1]. Here the most important plots are presented. For further plots, see Appendix B.

As it can be seen in Figure 4, the Bogacki-Shampine method was the least accurate and performed the worst, as observed in Figure 5. It required about 20 times more steps than the higher order methods with a tolerance of 10^{-4}. Figure 5 also shows that the Cash-Karp method provided the broadest mesh and the highest dt_{mean}, therefore the best performance overall. Another observation is that the step size of both the Cash-Karp and Fehlberg methods differ mainly at the higher values, while the step size for the Dormand-Prince method is less amplified. A last remark is that also the Dormand-Prince method scored the higher $\text{adapt}_{\text{mean}} = 1.3$, while the others remained at $\text{adapt}_{\text{mean}} = 1$.

To conclude, Figure 7 shows that the modified right-hand side implementation performs slightly better than the root-finding method. Clearly, it captures the same step size evolution while avoiding the sudden drops located at the non differentiability points.

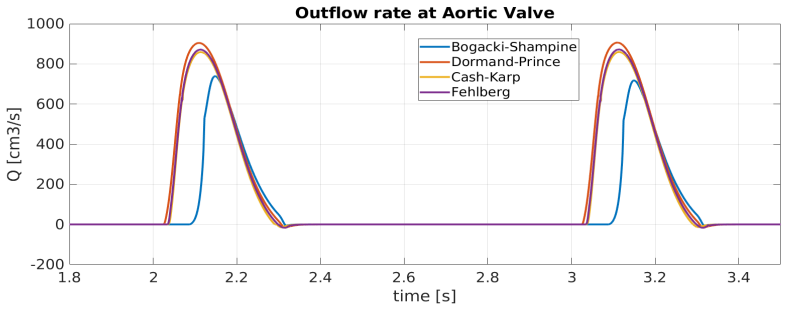

Figure 4: Comparison of numerical solutions for the flow rate in AV (Aortic valve).

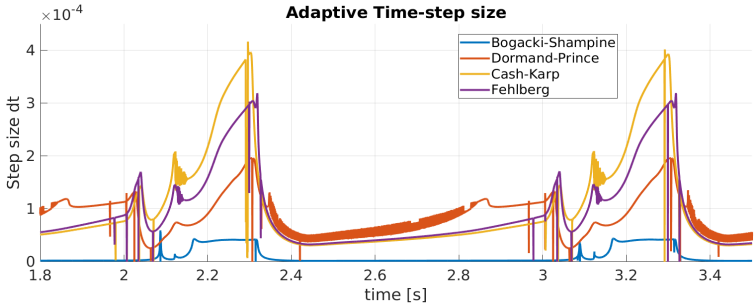

Figure 5: Time step size evolution for the four methods. The drops in step size are due to the crossing of points of non-differentiability.

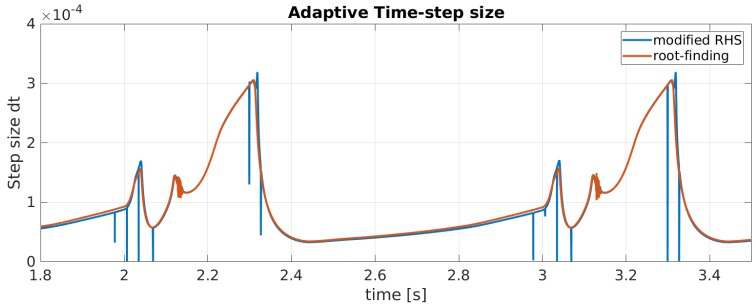

Figure 6: Evolution of the step size with Andersson-Björck method and the *smoothed* right-hand side, with $k = 8$ and both solved using the Fehlberg method.

5 Graphical Visualization and Data

The visualization of the most important parameters has been performed by taking a frame of two heartbeats and for the following values, taken inside the heart: pressure, volume and flow rate, opening coefficients of valves and pumping power (see figures 11, 12, 13, 14 and 15 in Appendix C).

Specifically, the heart's pumping power is represented as pressure-volume relation, expressing therefore the effect of reduced elasticity by applying Suga et al's variable elastance model [8].
To represent the effect of different working conditions of the system, the possibility to input different values of heart rate and elasticity has been added.
Furthermore, the opening coefficients of the valves are plotted, in order to highlight their importance for the functionality of the system, and the phases of their opening and closing cycle, as described by T. Korakianitis and Y. Shi in their study [8].
The use of data taken from medical literature [5] allows for a comparison of the results obtained in this study with medical observations: for instance, the most significant heart rates of 60, 160 and 200 bpm (respectively representing rest, physical activity and maximum) are taken into account to show the changes in the plots, while the values considered for the elasticity are 0.2, 0.5 and 1.0.

6 Results and Conclusions

The problem induced by the non differentiability points has been solved through both Anderson-Björck algorithm and the modification of the right-hand side of the system. The latter has shown slightly better results, namely the absence of sudden drops in step size which can be observed in the prior one.

The implementation of Fehlberg method with Andersson-Björck has proven to be more than 7 times faster than MATLAB's well-known *ode45* integrator. Besides, the implementation of automatic step size control has enabled an effective and efficient way to bound the discretization error of the solution.

Eventually, the graphical visualization shows not only the periodic behavior of the system, but also the changes in the behavior of the variables introduced by different values of heart rate (in bpm) and elasticity:

- Pressure in heart chambers and outflow at respective valves increase with augmented heart rate
- Volume of heart chambers decreases with increased heart rate
- The behavior of the opening coefficients *smoothens out* for augmented heart rate
- The pumping power (in Appendix C, figure 15 of the left ventricle) decreases with decreased elasticity, as expected from clinical observations.

References

[1] P. Bogacki and L.F. Shampine. "A 3(2) pair of Runge - Kutta formulas". In: *Applied Mathematics Letters* 2.4 (1989), pp. 321–325. ISSN: 0893-9659. DOI: https://doi.org/10.1016/0893-9659(89)90079-7. URL: https://www.sciencedirect.com/science/article/pii/0893965989900797.

[2] J. R. Cash and Alan H. Karp. "A Variable Order Runge-Kutta Method for Initial Value Problems with Rapidly Varying Right-Hand Sides". In: *ACM Trans. Math. Softw.* 16.3 (Sept. 1990), pp. 201–222. ISSN: 0098-3500. DOI: 10.1145/79505.79507. URL: https://doi.org/10.1145/79505.79507.

[3] J.R. Dormand and P.J. Prince. "A family of embedded Runge-Kutta formulae". In: *Journal of Computational and Applied Mathematics* 6.1 (1980), pp. 19–26. ISSN: 0377-0427. DOI: https://doi.org/10.1016/0771-050X(80)90013-3. URL: https://www.sciencedirect.com/science/article/pii/0771050X80900133.

[4] E. Fehlberg. *Low-order classical Runge-Kutta formulas with step size control and their application to some heat transfer problems.* 315. NASA Technical Report, 1969, pp. 1–13.

[5] Luca Formaggia, Alfio Quarteroni, and Alessandro Veneziani. *Cardiovascular Mathematics: Modeling and simulation of the circulatory system.* Vol. 1. Springer Science & Business Media, 2010.

[6] S. Galdino. "A family of regula falsi root-finding methods". In: 2011.

[7] Ernst Hairer, Syvert Norsett, and G. Wanner. *Solving Ordinary Differential Equations I: Nonstiff Problems.* Vol. 8. Jan. 1993. ISBN: 978-3-540-56670-0. DOI: 10.1007/978-3-540-78862-1.

[8] Theodosios Korakianitis and Yubing Shi. "Numerical simulation of cardiovascular dynamics with healthy and diseased heart valves". In: *Journal of biomechanics* 39.11 (2006), pp. 1964–1982.

[9] Fuyou Liang et al. "Multi-scale modeling of the human cardiovascular system with applications to aortic valvular and arterial stenoses". In: *Medical & biological engineering & computing* 47.7 (2009), pp. 743–755.

[10] Alfio Quarteroni, L Formaggia, and A Veneziani. "Cardiovascular mathematics". In: *Proceedings of the International Congress of Mathematicians.* Vol. 1. European Mathematical Society Madrid, Spain. 2006, pp. 479–512.

A Alternative adaptive step size

A further step size control is implemented in order to avoid hard fluctuations of the adaptive time-step as an alternative to using the control parameters $f_{\max}$ and $f_{\min}$. This adaptive step size control also follows the goal of tracking the local discretization error. In contrast, it maintains a fixed step size for some intervals of time, creating a hybrid between a fixed mesh and the aforementioned implementation which allows the control of the discretization error. It was expected to be more efficient, however by adjusting the parameters properly, one can see that it is basically a rounding down of the previous implementation.

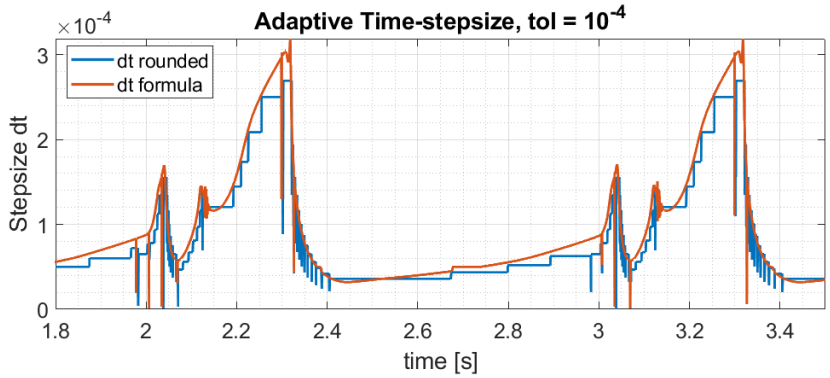

Figure 7: Comparison of the two versions of adaptive time step.

To see the implementation, see the code.

B Comparison of methods

In this Appendix the comparison plots for the other heart flow rates, following Fig. 4 are included. As discussed before, the solution from the Bogacki-Shampine method differs the most from the others. This is a coherent result, since it is a lower order method. The other methods provide very similar solutions, being the Dormand-Prince method the one who differs the most.

Furthermore, Table 1 is provided, which captures the values of the diagnostic parameters for the different methods.

Parameters	Bogacki-Shampine	Dormand-Prince	Cash-Karp	Fehlberg	modified RHS
dt_{mean}	$3.00 \cdot 10^{-6}$	$7.10 \cdot 10^{-5}$	$5.92 \cdot 10^{-5}$	$6.14 \cdot 10^{-5}$	$6.39 \cdot 10^{-5}$
$bjoerck_{mean}$	1.86	3	4.40	2.64	-
$adapt_{mean}$	1.00	1.30	1.00	1.00	1.00

Table 1: Values of the diagnostic parameters for the different methods.

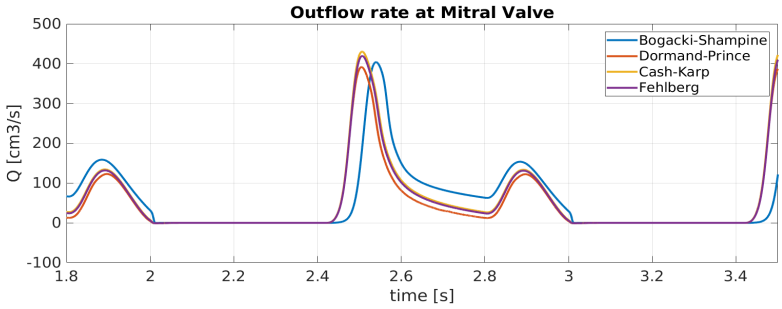

Figure 8: Comparison of numerical solution for flow rate in MV (Mitral valve).

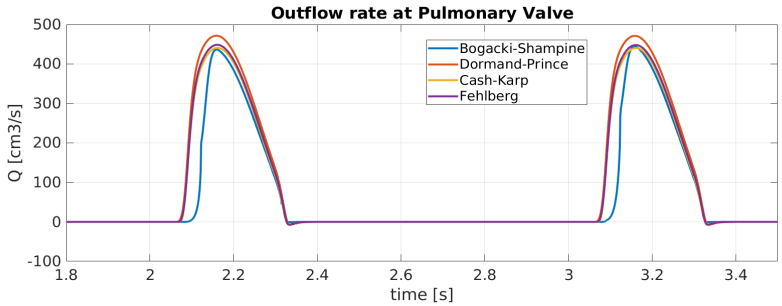

Figure 9: Comparison of numerical solution for flow rate in PV (Pulmonary valve).

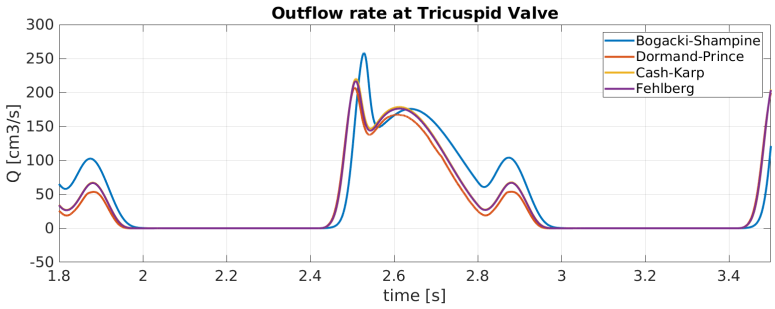

Figure 10: Comparison of numerical solution for flow rate in TV (Tricuspid valve).

C Relevant plots

The following plots are taken from the graphical user interface developed using MATLAB's *guide* tool (which will be replaced in more recent versions by the *AppDesigner* tool).
They show a side by side comparison of the behavior of pressure, volume, flow rate, opening coefficient of mitral valve and pumping power for the most significant values of heart rate and elasticity.

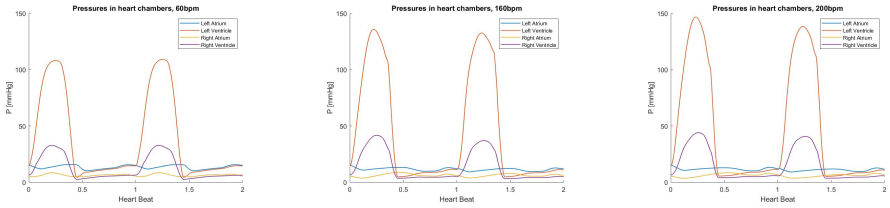

Figure 11: Pressure inside the heart, measured for two heartbeats at, respectively, 60 (rest), 160 (average during marathon) and 200 (maximal) bpm.

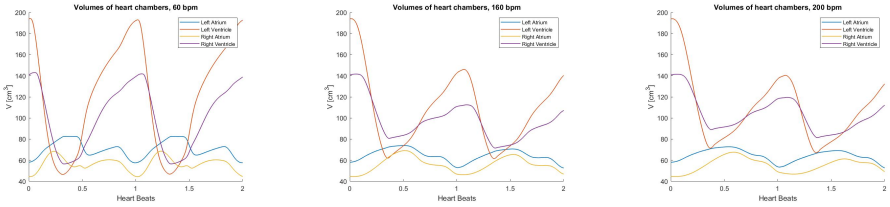

Figure 12: Volume inside the heart, measured for two heartbeats at, respectively, 60 (rest), 160 (average during marathon) and 200 (maximal) bpm.

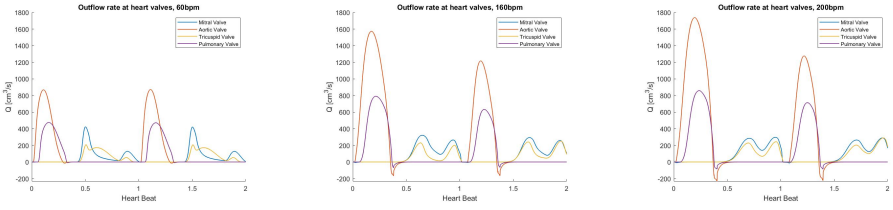

Figure 13: Flow rate at heart valves, measured for two heartbeats at, respectively, 60 (rest), 160 (average during marathon) and 200 (maximal) bpm.

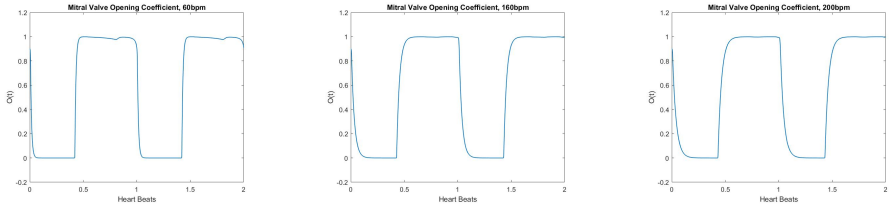

Figure 14: Opening coefficient of mitral valve, measured for two heartbeats at, respectively, 60 (rest), 160 (average during marathon) and 200 (maximal) bpm.

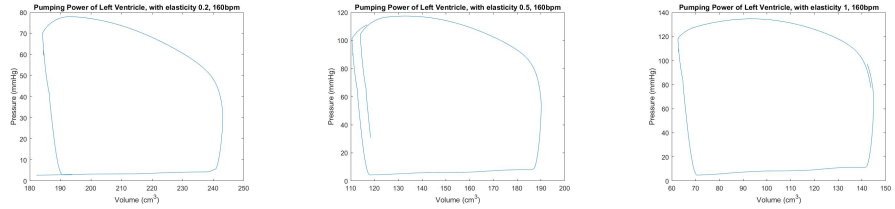

Figure 15: Pumping power of left ventricle at heart rate of 160 bpm for elasticity values of, respectively, 0.2, 0.5, 1.0.